

Wide frequency phonons manipulation in Si nanowire by introducing nanopillars and nanoparticles

Yatao Li(李亚涛), Yingguang Liu(刘英光), Xin Li(李鑫), Hengxuan Li(李亨宣), Zhixiang Wang(王志香), and Jiuyi Zhang(张久意)

Citation: Chin. Phys. B, 2024, 33 (**4**): 046502. DOI: 10.1088/1674-1056/ad0290
Journal homepage: http://cpb.iphy.ac.cn; http://iopscience.iop.org/cpb

What follows is a list of articles you may be interested in

Phonon transport properties of Janus Pb_2XAs (X = P, Sb, and Bi) monolayers: A DFT study

Jiaxin Geng(耿嘉鑫), Pei Zhang(张培), Zhunyun Tang(汤准韵), and Tao Ouyang(欧阳滔)
Chin. Phys. B, 2024, 33 (**4**): 046501. DOI: 10.1088/1674-1056/ad2260

Transport properties of CrP

Xuebo Zhou(周学博), Ping Zheng(郑萍), Wei Wu(吴伟), Yu Sui(隋郁), and Jianlin Luo(雒建林)
Chin. Phys. B, 2023, 32 (**7**): 076501. DOI: 10.1088/1674-1056/acc80c

Molecular dynamics study on the dependence of thermal conductivity on size and strain in GaN nanofilms

Ying Tang(唐莹), Junkun Liu(刘俊坤), Zihao Yu(于子皓), Ligang Sun(孙李刚), and Linli Zhu(朱林利)
Chin. Phys. B, 2023, 32 (**6**): 066502. DOI: 10.1088/1674-1056/acbf26

Effects of phonon bandgap on phonon-phonon scattering in ultrahigh thermal conductivity ϑ-phase TaN

Chao Wu(吴超) and Chenhan Liu(刘晨晗)
Chin. Phys. B, 2023, 32 (**4**): 046502. DOI: 10.1088/1674-1056/acb201

Influence of surface scattering on the thermal properties of spatially confined GaN nanofilm

Yang Hou(侯阳), Lin-Li Zhu(朱林利)
Chin. Phys. B, 2016, 25 (**8**): 086502. DOI: 10.1088/1674-1056/25/8/086502

SPECIAL TOPIC — Heat conduction and its related interdisciplinary areas

Wide frequency phonons manipulation in Si nanowire by introducing nanopillars and nanoparticles

Yatao Li(李亚涛), Yingguang Liu(刘英光)†, Xin Li(李鑫), Hengxuan Li(李亨宣), Zhixiang Wang(王志香), and Jiuyi Zhang(张久意)

Hebei Key Laboratory of Low Carbon and High Efficiency Power Generation Technology, North China Electric Power University, Baoding 071003, *China*

(Received 7 August 2023; revised manuscript received 20 September 2023; accepted manuscript online 12 October 2023)

The combination of different nanostructures can hinder phonons transmission in a wide frequency range and further reduce the thermal conductivity (TC). This will benefit the improvement and application of thermoelectric conversion, insulating materials and thermal barrier coatings, etc. In this work, the effects of nanopillars and Ge nanoparticles (GNPs) on the thermal transport of Si nanowire (SN) are investigated by nonequilibrium molecular dynamics (NEMD) simulation. By analyzing phonons transport behaviors, it is confirmed that the introduction of nanopillars leads to the occurrence of low-frequency phonons resonance, and nanoparticles enhance high-frequency phonons interface scattering and localization. The results show that phonons transport in the whole frequency range can be strongly hindered by the simultaneous introduction of nanopillars and nanoparticles. In addition, the effects of system length, temperature, sizes and numbers of nanoparticles on the TC are investigated. Our work provides useful insights into the effective regulation of the TC of nanomaterials.

Keywords: resonant structure, nanoparticles, nanopillars, phonon transport, thermal conductivity

PACS: 65.80.–g, 63.22.–m, 44.10.+i, 31.15.xv **DOI:** 10.1088/1674-1056/ad0290

1. Introduction

Many important applications and devices such as thermoelectric conversion, thermal barrier coatings and insulating materials need to hinder phonon transport to further reduce TC.[1–4] Nanostructures have been widely used in the design of low TC materials, and the frequency range of phonons that significantly contributes to heat transport in nanostructured materials is generally in the sub-terahertz to tens of terahertz.[5] From a spectral point of view, the key question in obtaining low TC materials is how to suppress phonon transmission over a wider frequency range.[6,7] However, a single nanostructure can only control or influence phonons within a certain frequency range and cannot suppress phonons at all frequencies to achieve extremely low TC.

Therefore, in order to further decrease the TC, many scholars have combined different nanostructures with other scattering sources to inhibit phonons transport in a wider frequency range. For example, Liu *et al.*[8] further significantly reduced the TC by embedding nanoparticles in the Si/Ge superlattice, which was mainly attributed to the fact that nanoparticles enhanced the scattering of middle-frequency phonons in the superlattice on the basis that most of the high-frequency phonons were scattered by the interfaces. Chen *et al.*[9] showed that Si/Ge superlattices combining point defects and abrupt boundaries can break the TC limit of alloying. This structure can scatter middle and high frequency phonons through point defects and abrupt boundaries, respectively. Similarly, experimental work[10] by using a combination of embedded nanoparticles, impurities, and sintered interfaces into material has yielded very low TC, which is attributed to the efficient scattering of phonons by these multiscale structures in a wider frequency range. It should be noted that the above studies are based on phonon's particle nature to enhance the scattering of middle and high frequency phonons. The disadvantage of this approach is that it has a weak influence on low-frequency phonons, which also have a non-negligible contribution to the TC,[11–13] thus limiting the further reduction in TC.

In contrast to the above works, more and more studies focus on using phonons wave nature to suppress low frequency phonons transport. The phonon resonance is a typical wave behavior, which can reduce the phonon group velocity and lifetime and produce phonon mode localizations and hybridization to decrease TC.[14,15] Therefore, the combination of resonant structures and other scatters can achieve phonon transport suppression in the full frequency range. For example, Wang *et al.*[16] reported that screw dislocations can enhance the anharmonicity of high-frequency phonons, while resonant structures can decrease the group velocity and relaxation time of low-frequency phonons. They can cooperatively inhibit phonon's transport at all frequencies in SNs. Xiong *et al.*[17] demonstrated that combining the designed resonant structure with alloying can result in extremely low TC of SNs. This is because the resonance structure causes the resonance effect of

†Corresponding author. E-mail: yingguang266@126.com

© 2024 Chinese Physical Society and IOP Publishing Ltd

low-frequency phonons, which reduces the group velocity and mean free path of phonons below 4 THz, while alloy scattering hinders the propagation of high-frequency phonons. Similarly, Liang *et al.*[18] showed that the surrounded fins and Ge dopants in SNs can effectively inhibit the transmission of low-frequency phonons and high-frequency phonons, respectively.

Although local resonance and scattering of phonons can suppress the transport of full frequency phonons, it is important to note that the mere combination of resonant structures and scatters does not necessarily lead to a decrease in TC because the introduction of phonon scatters will reduce the local resonance of phonons. For example, Wang *et al.*[19] investigated the effect of introducing vacancy defects, mass mismatch and alloy disorder into the side band of graphene nanojunction on phonon resonance mechanism, showing that various defects can weaken resonance hybridization and thus improve TC. Similarly, Li *et al.*[20] showed that the phonon resonant effect caused by the resonant pillars of Si-membranes can significantly reduce the TC of the Si-membranes, but the introduction of vacancies at the interface between resonant pillars and the base material decoupled the hybridization of the resonant mode and the propagating phonons at intermediate frequency, thus improving the TC of the resonant structure.

From the above analysis, we know that the combination of resonant structures and scatters can be very beneficial for the decrease of TC, however, the interaction between them may weaken the heat conduction inhibition effect. Thus, in order to avoid weakening phonons resonance effect of introducing scatterers and realize the synergistic effect between phonons scattering and resonant mechanisms, it is crucial to reasonably select the scattering source and resonant structure. Therefore, in this paper, we propose to rationally introduce resonant nanopillars and nanoparticles to reduce the TC of nanowires. The effects of nanoparticles and resonant nanopillars on the TC of nanowire are simulated by NEMD. By calculating the phonon spectral heat flux, dispersion relations and participation ratios, the heat transport mechanisms are deeply analyzed.

2. Model and computational methodology

2.1. Geometric model

All models are created in the ⟨100⟩ orientation using the LAMMPS code.[21] Figures 1(a)–1(d) show the simulation structures of SN, Si nanowire embedded with Ge nanoparticles (SN-PAR), Si nanowire with two-sided nanopillars (SN-PIL), and Si nanowires with both Ge nanoparticles and nanopillars (PAR-PIL). As shown in Fig. 2, the geometrical sizes of the four periodic structures are demonstrated by taking the smallest cell structure of PAR-PIL as an example. The main body of the minimum cell structure is a cube with a side length $L_a = 3.26$ nm. The cross section of the branches is a square with a side length $L_b = 1.63$ nm and its height is set to $L_h = 1.63$ nm. The two branches on either side have the same size and are both located in the middle of the square. Ge nanoparticles of diameter D are embedded in the center of the body.

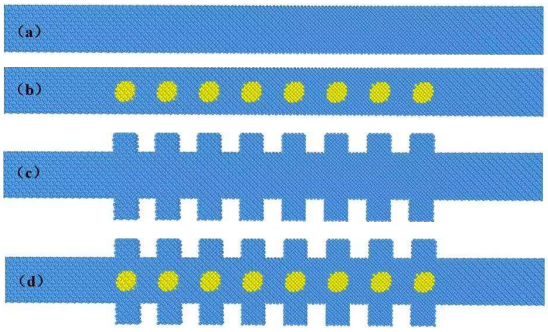


Fig. 1. Schematic diagram of the four structures: (a) Si nanowire, (b) Si nanowire with Ge nanoparticles, (c) Si nanowire with nanopillars, (d) Si nanowire with both nanopillars and Ge nanoparticles.

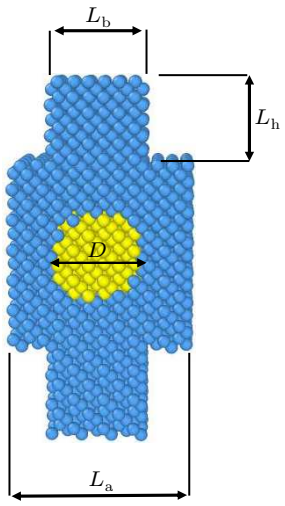


Fig. 2. The geometric size of the minimum cell structure.

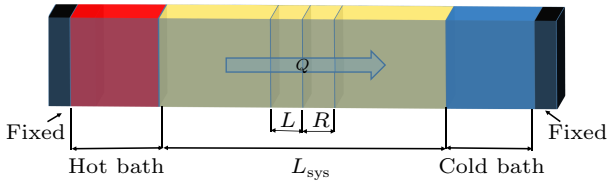


Fig. 3. Schematic diagram of the NEMD simulation.

2.2. Computational methodology

The TC of all models is calculated in LAMMPS software using the NEMD method. The interactions between atoms are described by the Tersoff potential,[22] which is widely used to calculate the thermal properties of Si–Ge materials. The schematic diagram of the NEMD simulation is shown in Fig. 3, the hot and cold baths are both set to be 16.0 nm. Fixed boundary condition is used in the X-direction, and the atoms at both ends in the range of 1 nm are set as fixed layers. Periodic

boundary conditions are used for the rest of the directions with a vacuum region of 8 conventional unit cells surrounding the Si nanowire, which is larger than the cutoff radius of atomic interactions. The temperatures of the hot and cold baths are set to be $T_0+\Delta T/2$ and $T_0-\Delta T/2$ by a Langevin thermostat, where T_0 is the initial temperature of the system and ΔT is the temperature difference between the hot and cold baths. The time step is set to be 1 fs. First, in the NPT ensemble, the system was relaxed for 5×10^6 time steps at zero pressure and a specific temperature. Subsequently, the optimized structure was obtained and the NVT for 1×10^6 time steps was performed to give the system a uniform energy distribution state at a desired temperature. After system equilibration, a temperature gradient was generated in the system using a Langevin thermostat and the system was placed under NVE for 1×10^6 time steps to obtain the heat flux. Figure 4 shows the temperature distribution in homogeneous SN after state stabilization, the temperature jump near the hot and cold bath can be clearly seen in the short finite length model. Previous studies which calculate temperature gradient always remove the jump part and fit only the intermediate linear part. However, the study by Li *et al.*[23] showed that the temperature jump, also known as ballistic thermal resistance, is a physical phenomenon due to the ballistic transport of some phonons, which should not be excluded in the temperature gradient fitting process. Therefore, the TC is calculated from Fourier's law by the temperature difference ΔT

$$\kappa=-\frac{J}{W\cdot d\cdot\dfrac{\Delta T}{L_{\rm sys}}}, \tag{1}$$

where J is the heat flow, W is the substrate width, d is the substrate thickness,[24,25] $L_{\rm sys}$ corresponds to the system length and temperature difference $\Delta T=40$ K.

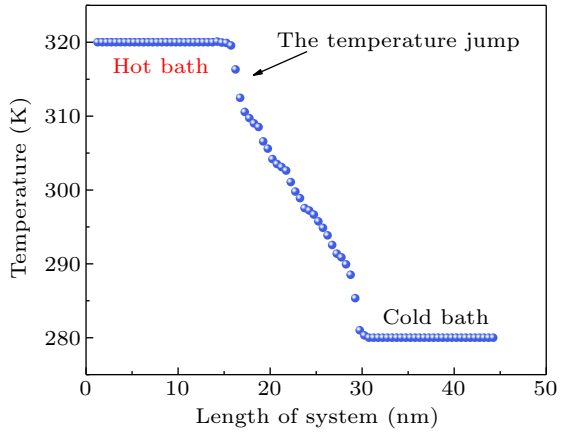


Fig. 4. The temperature distributions in homogeneous Si nanowire.

According to the method developed by Sellan *et al.*,[26] TC with finite sample length in NEMD simulation can be obtained by fitting extrapolation. In order to improve the extrapolation accuracy of fitting, Taylor series expansion is performed on the complex function composed of length dependent TC and $1/L$, and the expansion is truncated to the second-order[27,28]

$$\frac{1}{\kappa(L)}=\frac{1}{\kappa_0}+\frac{\alpha}{L}+\frac{\beta}{L^2}, \tag{2}$$

where $\kappa(L)$ is the TC obtained by NEMD simulations for the sample with length L. κ_0 corresponds to the extrapolated TC with α and β the extrapolation coefficients.

The spectral heat flows are obtained based on the calculation method used by Saeaeskilahti *et al.*[29–31] As shown in the schematic of the NEMD simulation (Fig. 3), the heat flowing from the L-group atoms to the R-group atoms can be calculated as

$$q_{i\to j}(\omega)=-\frac{2}{\omega t}\sum_{\alpha,\beta\in(x,y,z)}{\rm Im}\left\langle\tilde{v}_i^{\alpha}(\omega)^{*}K_{ij}^{\alpha\beta}\tilde{v}_j^{\beta}(\omega)\right\rangle, \tag{3}$$

here, ω represents the angular frequency, t is the simulation time and $K_{ij}^{\alpha\beta}$ is the second-order interatomic force constant. $\tilde{v}_i^{\alpha}(\omega)$ and $\tilde{v}_j^{\beta}(\omega)$ represent the discrete Fourier-transformed velocities of atoms i in direction α and atoms j in direction β, respectively. By summarizing the atoms in each subset of two adjacent atom subsets L and R (Fig. 1), the spectral heat flux at the intermediate interface can be obtained by

$$q(\omega)=\frac{1}{A}\sum_{i\in L}\sum_{j\in R}q_{i\to j}(\omega). \tag{4}$$

Phonon density of states (PDOS) can reflect the changes in the internal vibration mode of the system after being affected by external factors, and give a lot of important microscopic information. By performing the Fourier transform of the velocity autocorrelation function of each atom, the PDOS can be obtained as [32]

$${\rm PDOS}(\omega)=\frac{1}{\sqrt{2\pi}}\int{\rm e}^{-{\rm i}\omega t}\left\langle\sum_{j=1}^{N}\boldsymbol{v}_j(t)\boldsymbol{v}_j(0)\right\rangle, \tag{5}$$

where $\boldsymbol{v}_j(0)$ is the average velocity vector of a particle j at initial time, $\boldsymbol{v}_j(t)$ is its velocity at time t, and ω is the vibration wave number.

In order to better comprehend the influence of phonons activities on the TC of the system, we calculate phonons participation ratios (PPRs) of different structures according to the following formula:[33]

$${\rm PPR}(\omega)=\frac{1}{N}\frac{\left[\sum_i{\rm PDOS}_i(\omega)^2\right]^2}{\sum_i{\rm PDOS}_i(\omega)^4}, \tag{6}$$

where ${\rm PDOS}_i(\omega)$ is the PDOS of the i-th atom with frequency ω, and N is the total number of atoms.

3. Results and discussion

The relationship between TC and the length of the four structures at room temperature was first investigated. Due to the size effects,[20,34] the TC of each sample increased with the increase of system length. In order to obtain the TC of infinitely long samples (also known as intrinsic TC) with limited computational resources, Eq. (2) was applied to fit extrapolations of the TC obtained from the NEMD simulations for samples of finite length. The samples with ultra-short lengths were discarded in the quadratic fitting process[35] and the values of long samples with maximum lengths up to 417 nm were used to improve the extrapolation accuracy of TC. As shown in Fig. 5, the TCs of the four infinite structures predicted by TC extrapolation are 85.39 $W{\cdot}m^{-1}{\cdot}K^{-1}$, 18.30 $W{\cdot}m^{-1}{\cdot}K^{-1}$, 15.29 $W{\cdot}m^{-1}{\cdot}K^{-1}$ and 6.95 $W{\cdot}m^{-1}{\cdot}K^{-1}$, respectively. This first demonstrates that the introduction of GNPs and nanopillars can significantly reduce the TC of SN, but nanopillars and GNPs lead to different degrees of reduction in TC, as they introduce different phonons transport mechanisms.

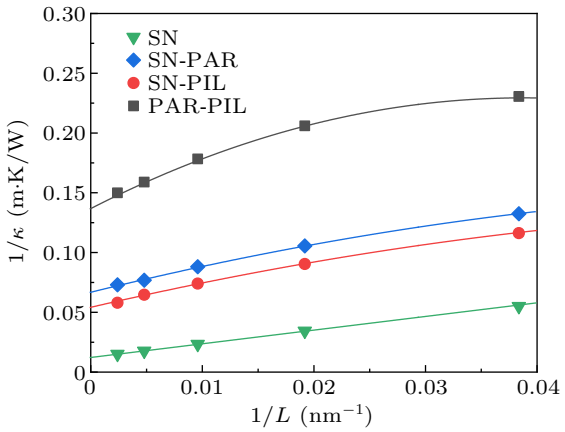


Fig. 5. The extrapolation of TC based on Eq. (2) for the four structures.

In order to quantitatively analyze the different phonons transport mechanisms, the $q(\omega)$ of SN, SN-PAR, SN-PIL and PAR-PIL are obtained by calculating the contribution of phonons of different frequencies to heat transport, as shown in Fig. 6. Compared with the value of $q(\omega)$ for SN, it can be seen that the embedded GNPs lead to a significant reduction of $q(\omega)$ for SN-PAR in the middle and high frequency ranges. This can be easily understood that the embedded GNPs as scattering sources enhance the scattering of middle and high frequency phonons.[8] However, the value of $q(\omega)$ corresponding to phonons frequencies lower than 2.5 THz is basically unchanged in these two structures. This is because, in the process of thermal transport, low frequency phonons with long mean free path pass through GNPs in the way of ballistic transport and are not scattered.[36,37]

It also can be seen from Fig. 6 that due to the resonance hybridization effect of the nanopillars, $q(\omega)$ of SN-PIL in the whole spectrum is lower than SN. However, the reduction of $q(\omega)$ of SN-PIL is different from that of SN-PAR, firstly, the reduction degree in the mid-high frequency range is not as significant as that of SN-PAR. This suggests that although the introduction of nanopillars introduces additional phonon-boundary scattering, it is weaker than that of internal scattering induced by nanoparticles. The second difference is that $q(\omega)$ of SN-PIL decreases more significantly than that of SN-PAR in the frequency range below 2.5 THz. This is attributed to the fact that the nanopillars reduce the group velocity, relaxation time and mean free path of phonons through the resonance hybridization effect, which is more effective in suppressing low frequency phonons.[38–40] Notably, the simultaneous introduction of nanopillars and GNPs of SN leads to a significant reduction of $q(\omega)$ over the whole frequency range. This further demonstrates that phonon resonance and phonon scattering can complement each other to achieve synergistic inhibition of low and high frequency phonon transport.

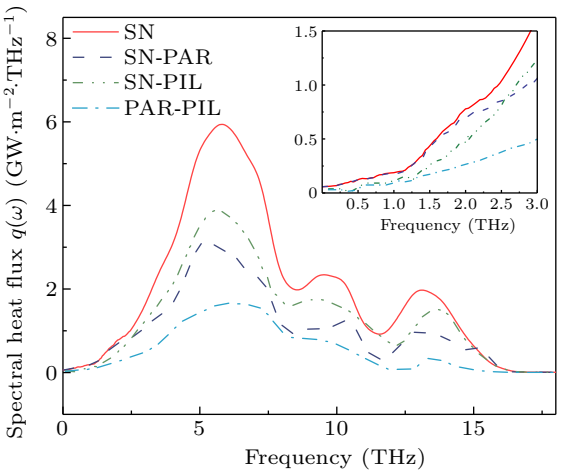


Fig. 6. Spectral heat flux of the four structures.

In order to elaborate the mechanism of TC reduction in more detail, phonon dispersion curves and group velocities of SN, SN-PIL, SN-PAR and PAR-PIL are calculated by the general utility lattice program (GULP) code[41] and the vibrational intrinsic modes of phonons are analyzed. Since local resonance of phonons which mainly occurs at low frequency, we focus on showing and analyzing dispersion below 3 THz. It can be seen from the dispersion curves, as shown in Figs. 7(a) and 7(d), that have large differences between different structures. Compared with SN, the dispersion curves of SN-PIL are almost constant, which is an evidence of phonon local resonance. The dispersion plot of SN-PAR shows that the embedding of GNPs has almost no effect on phonon patterns below 0.8 THz, but causes a lot of flattening of curves and phonon hybridization above 0.8 THz. This indicates that the embedding of nanoparticles will not only cause scattering of high-frequency phonons, but also resonance and hybridization of

low-frequency phonons. However, the frequency of affected resonance phonons is higher than that of nanopillars. The dispersion plots of PAR-PIL and SN-PIL are almost the same and compared with SN-PAR the heterogeneity caused by the nanoparticles in PAR-PIL disappears, which indicates that the nanopillars suppress the influence of nanoparticles on low frequency phonons when the nanoparticles and nanopillars are combined. We know that the flatness of the dispersion curve represents the decrease of the phonon group velocity, and the change of the group velocity of the corresponding structure can be intuitively observed in Figs. 8(a) and 8(d). As can be seen from the figure, both nanoparticles and nanopillars significantly reduce the group velocity of low-frequency phonons in a certain range based on the phonon resonance. But the two structures also reduce the group velocity of high-frequency phonons, which is mainly due to the hybridization of low-frequency resonant phonons to high-frequency phonons. In Fig. 8(d), no matter the high frequency optical branch or the low frequency acoustic branch, the group velocity of PAR-PIL is the lowest in the whole frequency range, which further proves that nanopillars and nanoparticles can jointly reduce TC of SN.

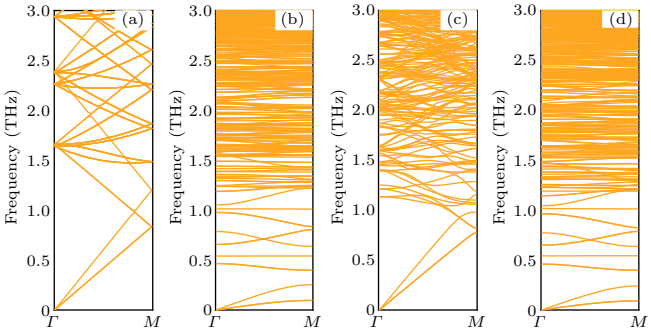


Fig. 7. Phonon dispersion of (a) SN, (b) SN-PIL, (c) SN-PAR and (d) PAR-PIL.

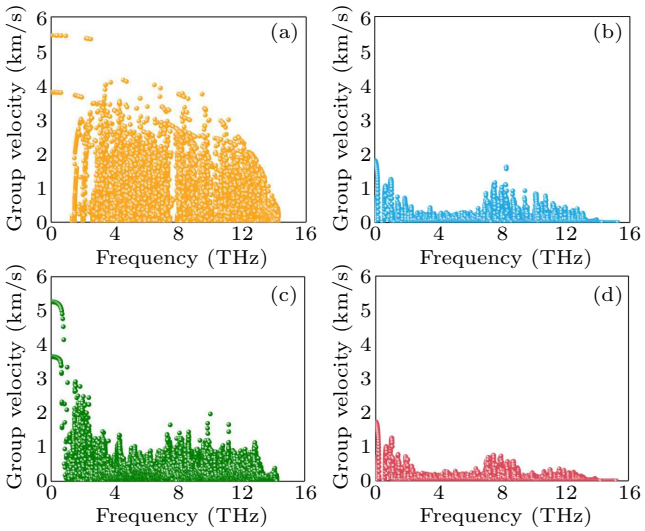


Fig. 8. Phonon group velocities of (a) SN, (b) SN-PIL, (c) SN-PAR and (d) PAR-PIL.

In order to further study the phonon transport behavior, we calculate the PPRs of SN, SN-PAR, SN-PIL and PAR-PIL, as shown in Fig. 9. It is known that smaller PPRs correspond to the stronger phonon localization, which leads to smaller TC. It can be seen that the introduction of nanoparticles mainly reduces the participation ratios of high-frequency phonons (8 THz–16 THz), while the introduction of nanopillars decreases the participation ratios of low-frequency phonons more (0 THz–5 THz). PAR-PIL combines precisely phonons localization in both SN-PAR and SN-PIL structures, and the PPRs value is the smallest in the whole frequency range. Therefore, compared with SN, SN-PAR, SN-PIL and PAR-PIL all exhibit different degrees of localization, and the localization degree of PAR-PIL is the most obvious. This is consistent with the lowest TC value of PAR-PIL.

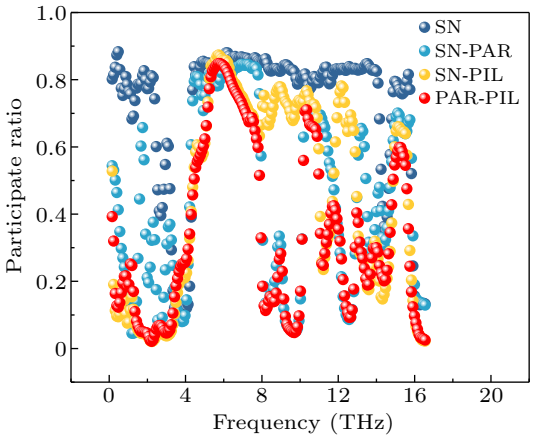


Fig. 9. Phonons participation ratios versus phonon frequency for SN, SN-PAR, SN-PIL and PAR-PIL.

The number and height of nanopillars are important factors affecting the heat transport of SNs, and previous studies[17,18] have fully concluded that the TC of SN decreases with increasing the number and height of nanopillars. This is due to the fact that higher and more nanopillars further reduce the phonon group velocity through the increase of phonon resonance hybridization. The TC is also closely related to the number and diameter of embedded GNPs,[8,42] so our main work in this section is to study the influence of the number and diameter of nanoparticles on the TC of PAR-PIL when the number of nanopillars remains unchanged. Figure 10 shows the variation of TC of PAR-PIL with the diameters and numbers of GNPs, it can be seen that the TC shows a monotonic decreasing trend with the nanoparticle number and diameter, respectively. As the diameter and the number of GNPs increase, the TC decreases significantly and the maximum reduction is up to 55%. The reduction in TC can be easily explained that both the increase of nanoparticle number and size enhance phonon-interface scattering, thus leading to the reduction of TC.[42,43]

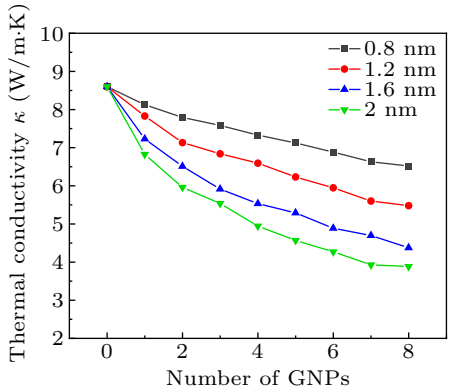


Fig. 10. Effect of diameter and number of GNPs on TC of SN-PIL.

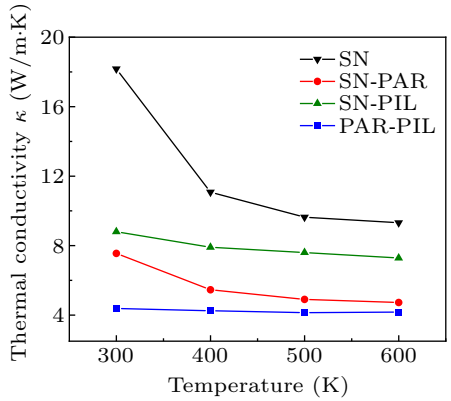


Fig. 11. Effects of temperature on TC of the four structures.

In addition, we explore the effect of temperature on TC. Figure 11 shows the variation of TC of SN, SN-PAR, SN-PIL and PAR-PIL with temperatures from 300 K to 800 K, and the four structures have obvious differences in temperature dependence. The TC of SN decreases with increasing temperature and exhibits a strong anharmonic effect. This is due to the dominance of Umklapp scattering in heat transport with increasing temperature,[44] resulting in a $1/T$ trend of TC versus temperature. The dependence of TC on temperature is smaller in SN-PAR and SN-PIL compared to the case of SN. One reason for the decreased temperature effect is that the placement of particles and pillars breaks the crystal structure and makes the material tend to be amorphous. One reason for the diminished temperature effect is that the introduction of nanopillars and nanoparticles disrupts the crystal structure and tends to amorphize the material. Another reason is due to the fact that the embedded GNPs scatter most of the middle and high frequency phonons, while the temperature increase can only make the fewer high frequency phonons in SN-PAR produce anharmonic properties and have a smaller effect on the TC. The variation of TC of SN-PIL with temperature is similar to that of SN-PAR, because resonance mainly blocks low-frequency phonons, while the high-frequency modes are only partially blocked and the anharmonicity can still disperse the remaining high-frequency phonons. It can be easily seen that PAR-PIL is insensitive to temperature and the combined effect of nanopillars and GNPs is an important reason for this phenomenon. This will facilitate the improvement of the thermoelectric properties of Si–Ge materials and their application in different temperature scenarios.

4. Conclusion and perspectives

The effects of nanopillars and GNPs on the thermal transport of SNs are investigated based on NEMD simulations. It is found that both nanopillars and GNPs can effectively block phonons transport and significantly reduce the TC. The analysis of spectral heat flux shows that GNPs reduce the TC mainly by scattering the middle and high frequency phonons, and have little effect on the low frequency phonons as they transport ballistically. The phonon dispersion relation and group velocity indicate that the nanopillars reduce the speed of the phonon group significantly and effectively block the heat transport of low frequency phonons through the resonance hybridization effect. The co-introduction of nanopillars and GNPs can synergistically regulate phonon transport in the full frequency range by complementing phonon resonance and phonon scattering to achieve extremely low TC. This indicates that the reasonable combination of different nanostructures can regulate phonon transport more effectively than the introduction of a single nanostructure. The reduction of TC caused by nanopillars and GNPs is closely related to the number and size of GNPs, the system length and temperature. The results show that the targeted structural design based on the particle and wave nature of phonons can more effectively hinder the transport of phonons and provide a feasible way to effectively regulate the TC of materials.

Acknowledgments

Project supported by the National Natural Science Foundation of China (Grant No. 52076080) and the Natural Science Foundation of Hebei Province of China (Grant No. E2020502011).

References

[1] Zhang P, Ouyang T, Tang C, He C Y, Li J, Zhang C X and Zhong J X 2020 *Chin. Phys. B* **29** 118401
[2] Zhao X and Jiang J W 2022 *Chin. Phys. B* **31** 126802
[3] Xu Y 2016 *Chin. Phys. B* **25** 117309
[4] Xu H H, Liu X Y, He Y H, Fan C, Du G, Sun A D, Han R Q and Kang J F 2010 *Chin. Phys. B* **19** 014601
[5] Hori T and Shiomi J 2018 *Sci. Technol. Adv. Mater.* **19** 10
[6] Cocemasov A I, Isacova C I and Nika D L 2018 *Chin. Phys. B* **27** 056301
[7] Zhang H G, Sun B, Hu S, Wang H Y, Cheng Y J, Xiong S Y, Volz S and Ni Y X 2020 *Phys. Rev. B* **100** 205418
[8] Liu Y G, Li Y T, Shen K B, Qiu Y J and Xie J 2023 *Int. J. Heat Mass Tranf.* **203** 123789
[9] Chen P X, Katcho N A, Feser J P, Li W, Glaser M, Schmidt O G, Cahill D G, Mingo N and Rastelli A 2013 *Phys. Rev. Lett.* **111** 115901

[10] Biswas K 2012 *Nature* **489** 414
[11] Zhou Y and Hu M 2016 *Nano. Lett.* **16** 6178
[12] Nakamura Y, Isogawa M, Ueda T, Amasaka S Y, Matsui H, Kikkawa J, Ikeuchi S, Oyake T, Hori T, Shiomi J and Sakai A 2015 *Nano Energy* **12** 845
[13] Hu S, Zhao C Y and Gu X 2022 *Chin. Phys. B* **31** 056301
[14] Davis B L and Hussein M I 2014 *Phys. Rev. Lett.* **112** 055505
[15] Hussein M I, Tsai C N and Honarvar H 2020 *Adv. Funct. Mater.* **30** 1906718
[16] Wang H Y, Cheng T J, Nomura M, Volz S, Donadio D, Zhang X H and Xiong S Y 2021 *Phys. Rev. B* **103** 085414
[17] Xiong S Y, Sääskilahti K, Kosevich Y A, Han H X, Donadio D and Volz S 2016 *Phys. Rev. Lett.* **117** 025503
[18] Liang Q, He Y L and Hung T C 2021 *Int. J. Heat Mass Transf.* **176** 121425
[19] Wang H Y, Cheng Y, Fan Z, Guo Y, Zhang Z, Bescond M, Nomura M, Ala-Nissila T, Volz S and Xiong S 2021 *Nanoscale* **13** 10010
[20] Li K, Cheng Y, Wang H, Guo Y, Zhang Z, Bescond M, Nomura M, Volz S, Zhang X and Xiong S 2022 *Int. J. Heat Mass Transf.* **183** 122144
[21] Plimpton S 1995 *J. Comput. Phys.* **117** 1
[22] Tersoff J 1989 *Phys. Rev. B* **39** 5566
[23] Li Z, Xiong S Y, Sievers C, Hu Y, Fan Z Y, Wei N, Bao H, Chen S D, Donadio D and Ala-Nissila T 2019 *J. Chem. Phys.* **151** 234105
[24] Cui L, Guo X, Yu Q, Wei G and Du X 2022 *Int. J. Heat Mass Transf.* **196** 123227
[25] Ma D, Wan X and Yang N 2018 *Phys. Rev. B* **98** 245420
[26] Sellan D P, Landry E S, Turney J E, McGaughey A J H and Amon C H 2010 *Phys. Rev. B* **81** 214305
[27] Wan Y, Xiong S, Ouyang B, Niu Z, Ni Y, Zhao Y and Zhang X 2019 *ACS Omega* **4** 4147
[28] Zaoui H, Palla P L, Cleri F and Lampin E 2016 *Phys. Rev. B* **94** 054304
[29] Sääskilahti K, Oksanen J, Tulkki J and Volz S 2014 *Phys. Rev. B* **90** 134312
[30] Sääskilahti K, Oksanen J, Volz S and Tulkki J 2015 *Phys. Rev. B* **91** 115426
[31] Ma Y L, Zhang Z W, Chen J G, Sääskilahti K, Volz S and Chen J 2018 *Carbon* **135** 263
[32] Li B W, Lan J H and Wang L 2005 *Phys. Rev. Lett.* **95** 104302
[33] Liang T, Zhou M, Zhang P, Yuan P and Yang D G 2020 *Int. J. Heat Mass Transf.* **151** 119395
[34] Tang Y, Liu J, Yu Z, Sun L and Zhu L 2023 *Chin. Phys. B* **32** 66502
[35] Dong H K, Fan Z Y, Shi L B, Harju A and Ala-Nissila T 2018 *Phys. Rev. B* **97** 094305
[36] Kang J S, Li M, Wu H, Nguyen H and Hu Y J 2018 *Science* **361** 575
[37] Sun Y, Zhou Y, Han J, Hu M and Liu W 2020 *J. Appl. Phys.* **127** 45106
[38] Chen X K, Liu J, Xie Z X, Zhang Y, Deng Y X and Chen K Q 2018 *Appl. Phys. Lett.* **113** 121906
[39] Giri A and Hopkins P E 2018 *Phys. Rev. B* **98** 045421
[40] Huang X, Ohori D, Yanagisawa R, Anufriev R, Samukawa S and Nomura M 2020 *ACS Appl. Mater. Inter.* **12** 25478
[41] Gale J D and Rohl A L 2003 *Mol. Simul.* **29** 291
[42] Kim W and Majumdar A 2006 *J. Appl. Phys.* **99** 084306
[43] Mingo N, Hauser D, Kobayashi N P, Plissonnier M and Shakouri A 2009 *Nano Lett.* **9** 711
[44] Liu Y G, Bian Y Q, Chernatynskiy A and Han Z H 2019 *Int. J. Heat Mass Transf.* **145** 118791